3 Integrating Modern Diagnostic Tools with Digital Engineering

Panos Diamantopoulos and Gerlig Widmann

3.1 Introduction to Applied Digital Technologies

3.1.1 Medical Imaging

Medical imaging is the creation of a visual representation of the human anatomy. It has been an important diagnostic tool since the discovery of X-rays by Roentgen in 1895. Techniques other than simple planar radiographs have become available during the last 50 years. These include, in historical order, radioisotope nuclear medicine (NM), ultrasound (US), computed tomography (CT), and magnetic resonance (MR) imaging. As a subject, it has grown enormously over the past few decades. One of the major developments has been the development of techniques for constructing images representing slices through three-dimensional (3D) objects. These techniques are called tomography and are based on the idea that an object may be constructed from projections. The theory of reconstruction from projections predates the construction of any actual scanner for computed tomography. It is generally accepted that the problem was first analyzed by Radon in 1917 [1]. An account of the method and the first system for reconstructing X-ray medical images probably originated from Russia [2, 3], although it is the work of Hounsfield in 1972 [4] that led to the first commercially developed system. It was the first system to produce section images of high quality and paved the way to tomographic and three-dimensional imaging techniques. The success of CT depended largely though on the development of a fast and accurate image reconstruction algorithm by Cormack in 1980 [5]. This, in turn, generated a general interest in reconstruction algorithms and digital imaging.

It is important to keep in mind that the data acquired by the system detectors represent spatial distribution of intensity. This distribution can be mathematically described as a two-dimensional (2D) function $f(x,y)$, where x and y are spatial coordinates and the value of f at any point (x,y) is proportional to the brightness or gray value of the data at that point. To create a digital image, a sampling process occurs that creates discrete finite picture elements (called pixels) and assigns to them both a location (x,y coordinates) and a color or gray value (f-value) (Fig. 3.1). This process is known as digital imaging or digitizing [6].

The picture elements are directly stored in the computer into a 2D matrix, also called an array or a frame, using analog-to-digital converters

P. Diamantopoulos
Medical 3D Printing Unit, Laboratory of Experimental Physiology, Medical School, University of Athens, Athens, Greece
e-mail: p.diamantopoulos@med.uoa.gr

G. Widmann (✉)
Department of Radiology, Medical University of Innsbruck, Innsbruck, Austria
e-mail: gerlig.widmann@i-med.ac.at

M. Rinaldi (ed.), *Implants and Oral Rehabilitation of the Atrophic Maxilla*,
https://doi.org/10.1007/978-3-031-12755-7_3

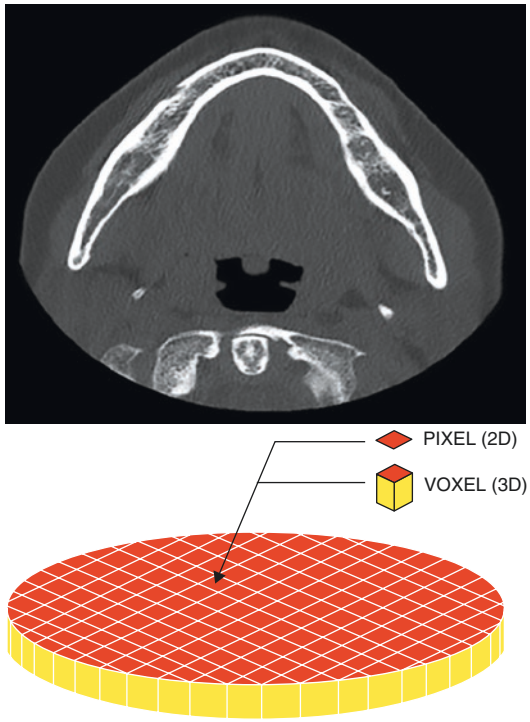

Fig. 3.1 An image slice is represented by pixels and voxels depicting the acquired spatial intensity in different shades of gray. The sum of pixels and voxels is known as resolution

(ADCs). Typically, a two-dimensional image is made up of M rows, each of N pixels. A value is assigned to each of them, representing either the integrated or the average image intensity across the pixel or a sampled value at the center of the pixel. A three-dimensional image is made up of K slices or planes each containing M rows, each of N pixels. The elements in this case are called voxels (volume elements). Pixels are invariably square, but voxels are not always cubic because it depends on the image thickness during image acquisition.

In general, a typical digital medical imaging system process includes (a) image digitization, (b) image storage, (c) image display, and (d) image processing and analysis. Digital radiographic systems present advantages in all these steps as well as dose reduction. However, it is a fact that most imaging data is presented in a two-dimensional black and white format. They are grayscale images without actual color. Multiple color, three-dimensional visualization can be achieved using the high-specification workstations accompanying the medical scanners. In this case, the applied colors are also artificial and are thus called pseudo-colors, with the intention of making intensity differences more apparent. Such weaknesses have often been limiting the application potential. In addition, medical scanners have generally been "closed systems," scanner to workstation, which offer limited or no external access to their data. Transferring data to external systems has been a particularly demanding task, requiring specific hardware, software, and special expertise. As a result, the potential of utilizing medical imaging information in other scientific domains, such as biomechanical engineering, has not yet been fully realized.

In maxillofacial surgery, 3D imaging using computed tomography (CT) or, most recently, cone-beam computed tomography (CBCT), has become an essential prerequisite for modern presurgical evaluation, treatment planning, digital engineering, and computer-guided surgery. A summary of the most important imaging aspects relevant to the maxillofacial practice is provided below:

3.1.1.1 Short Basics of CT and CBCT Technology

Computed Tomography (CT)

In CT, the subject is scanned using a helical rotating X-ray beam. Multislice detectors opposite to the X-ray beam record the information, which is transformed into digital images using filtered back projection or iterative reconstructive techniques. The volumetric data can be displayed in axial or multiplane image reconstructions. Furthermore, curved plane reconstructions including cross-sectionals and panoramic reconstructions as well as 3D reconstructions using volume rendering or cinematic volume rendering techniques are available. Modern CT scanners

are multifunctional, high-tech machines for diagnostics of the entire body. CT has become a diagnostic mainstay in acute medicine, trauma, and oncology.

Cone-Beam Computed Tomography (CBCT)

In CBCT, the subject is scanned using a 180–360° rotating beam-shaped X-ray, which is recorded by an opposite flat-panel detector to generate CT-like images [7]. Compared with CT scanners, CBCT machines are more compact and smaller and can be installed in dental offices. The scan range is limited to the head area, and there is no soft tissue imaging. However, CBCT has a high spatial resolution and an excellent bone image quality [8]. Due to the longer scan time, motion artifacts can be a possible source of errors.

3.1.1.2 Radiation Dose

Medical societies and legislative directives demand strict adherence to evidence-based imaging guidelines and patient's informed consent. Surgery and implant rehabilitation in the atrophic maxilla is a clear indication for CT/CBCT imaging. Dose management should follow the principle of "as low as reasonably achievable" (ALARA) and "as low as diagnostically acceptable" (ALADA) [9]. For benchmarking of CT radiation doses across institutions and scanners, diagnostic reference levels (DRLs) are provided by national radiological societies [7]. Regular excess of DRLs may attract local reviews and audits with the assistance of medical physicists. DRLs are given as phantom-based dose estimates such as the volume CT dose index, CTDIvol (mGy), and the dose length product, DLP (mGy × cm), which are documented in the Digital Imaging and Communications in Medicine (DICOM) dose report [8]. CTDIvol refers to the dose within one radiated slice (a nominal beam width) and considers the ratio of the nominal beam width and table feed (pitch). DLP is the product of CTDIvol and scan length. The effective dose (E) of an examination can be estimated using DLP and a conversion factor (k) ($E = k \times \text{DLP}$) [10]. Following the current International Commission on Radiation Protection (ICRP) 103 recommendations, a conversion factor of 0.0019 mSv/mGy × cm is used for CT of the head and 0.0051 mSv/mGy × cm for examinations of the head and neck area [11].

CBCT is erroneously considered a low-dose modality, based on comparisons of doses from CBCT with an extremely limited scan range and CT doses using head protocols. More recently, ultra-low-dose (CTDIvol <3 mGy) CT protocols have shown similar doses to CBCT. Since there is currently no standardized dose reporting in CBCT, comparisons of different scanners and protocols as well as comparisons to CT remain difficult [12].

Continuous efforts in dose saving and protocol optimization are pursued [13]. Iterative and model-based reconstructions may provide potential dose-saving options of up to 80% [7]. Organ-based dose modulation may reduce dose to the eye lenses by about 27–50% at equivalent CTDIvol, without reduction of image quality [14]. Published ALADA CT doses (CTDIvol) are: maxillofacial trauma 2.6 mGy [15, 16]; detection of the mandibular canal 1.74 mGy [17]; linear measurement accuracy for oral implant planning 0.29 mGy [18, 19]; fabrication of CAD models 0.99 mGy [20]; and image-guided surgery 0.76 mGy [21]. Future developments, such as artificial intelligence-assisted image reconstruction and photon-counting detectors have great potential in further dose savings. An example of ultra-low-dose CT and 3D cinematic rendering is displayed in Fig. 3.2.

3.1.1.3 Generic Imaging Protocols

The following generic protocols can be recommended (Table 3.1).

3.1.1.4 Accuracy of 2D and 3D Measurements

CT and CBCT may show similar accuracy for 2D and 3D measurements and similar accuracy of static and dynamic guided surgeries (Table 3.2) [22–31]. It is essential that head motion is avoided during the scan procedure. Translations of up to

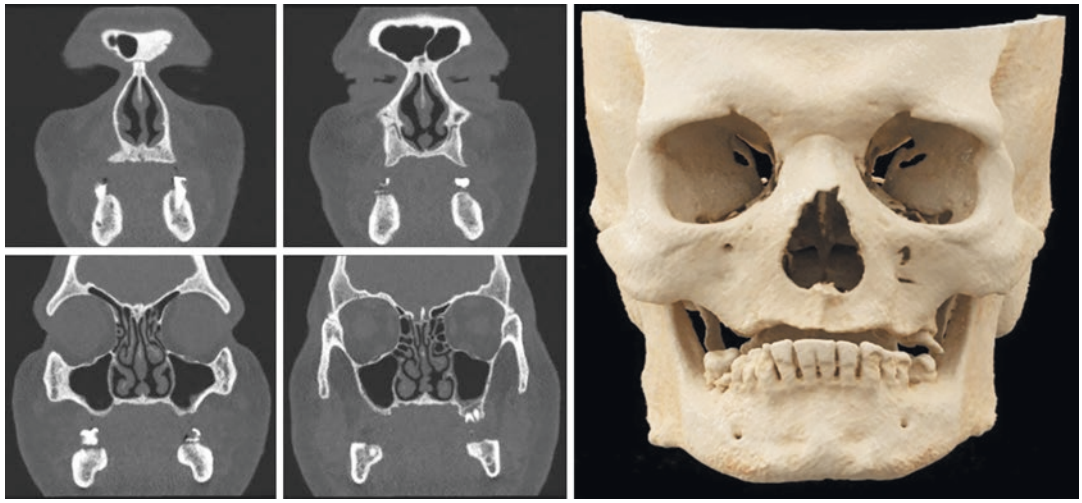

Fig. 3.2 Atrophic maxilla of a 35-year-old man (YOM) using ultra-low-dose CT at CTDIvol 2.34 mGy and DLP 37.47 mGycm (0.071 mSv) showing coronal reconstructions and 3D cinematic rendering (natural background radiation is 2.4 mSv per year)

Table 3.1 Generic CT and CBCT protocols

CT	CBCT
80–100 kV	120 kV
50–60 mAs	30–40 mAs
Rotation time 0.5–1 s	10–20 s
Voxel size 0.3 mm	Voxel size 0.09–0.2 mm

Table 3.2 Accuracy of CT and CBCT for surgical planning and guided surgery based on comparative studies [22–31]

	CT	CBCT
Measurement accuracy 2D (mean error)	0.06–0.54 mm	0.09–0.37 mm
Measurement accuracy 3D (mean error)	0.137	0.165–0.386 mm
Static guidance accuracy (mean lateral error tip)	1.1–1.6 mm	1.0–1.8 mm
Static guidance accuracy (mean angular error)	2.6–7.9°	2.7–6.5°
Dynamic guidance accuracy (mean lateral error tip)	1.3–1.7 mm	1.3–1.5 mm

5 mm and head rotation of even more than 2° may remain unnoticed since they may not display observable motion artifacts [32]. The longer the scan time and the less compliant patients are, the higher the risk of inaccuracies due to motion.

3.1.1.5 Image-Based Classification of Bone Quality

The revised Lekholm and Zarb classification categorizes the cortical bone according to thickness as "thick layer" or "thin layer" and the trabecular bone according to density as "dense," "medium density," or "low density" (see Table 3.3). This classification has a high reproducibility and efficiently distinguishes between the various combinations of the compact and trabecular bone [33, 34].

3.1.1.6 Digital Imaging and Communications in Medicine (DICOM)

The earliest digital medical imaging devices were proprietary in nature. There was no expectation that there would be a need to transfer digital images between devices, software applications, and scientific domains. The American College of Radiology/National Electrical Manufacturers Association (ACR-NEMA) standard published in 1985 was the first effort to develop an open standard. This was sponsored by the American College of Radiology (ACR) and the National Electrical Manufacturers Association (NEMA).

Table 3.3 Revised Lekholm and Zarb classification [33]

Type 1	An entirely homogeneous compact bone
Type 2a	A thick layer of the compact bone surrounds the core of the dense trabecular bone
Type 2b	A thick layer of the compact bone surrounds the core of the medium-density trabecular bone
Type 2c	A thick layer of the compact bone surrounds the core of the low-density trabecular bone
Type 3a	A thin layer of the compact bone surrounds the core of the dense trabecular bone
Type 3b	A thin layer of the compact bone surrounds the core of the medium-density trabecular bone
Type 4	A thin layer of the compact bone surrounds the core of the low-density trabecular bone

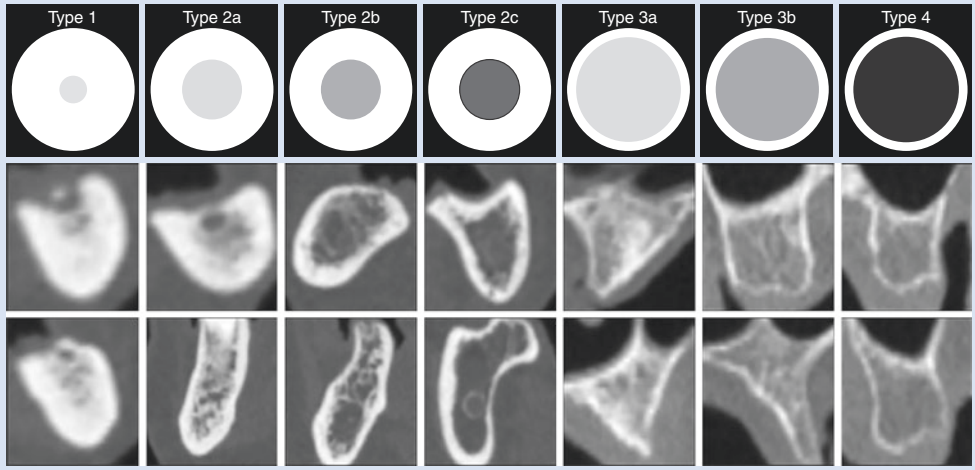

In 1993, a revised version was produced, namely, Digital Imaging and Communications in Medicine (DICOM), which, since then, has gradually become the standard image format for interoperability in the field of medical imaging.

3.1.2 Computer-Aided Design (CAD)

Computer-aided design (CAD) enables the development of a geometric model by electronic means and by drawing points, lines, curves, polygons, ellipses, etc. through a relevant software application. In general, CAD allows the production of virtual three-dimensional models and, in turn, designs, which are almost impossible to produce otherwise. Nowadays, there is a wide variety of modeling packages available for different applications. The most important areas are product design, virtual reality (VR), and real-time simulation. As the computer performance improves, these application areas begin to merge. There are still multiple formats utilized according to the application, but attempts are being made to establish standards for appropriate communication. The main problem is the mathematical representation of the surface, which is determined by software and hardware restrictions. It is important to note that for product design applications, the emphasis is on model accuracy, whereas in virtual environments (e.g., films, games), the ability to display models quickly is of primary importance.

The underlying theory of computer-aided design (CAD) is geometrical modeling. A geometric model is a three-dimensional description of an object. Such a description requires information on geometry, topology, and special features (such as tolerances, colors, textures). Geometry describes the exact shape and the position of each of the vertices, edges, and faces. The geometry of a vertex is its position in space as given by its (x,y,z) coordinates. Edges may be straight lines, circular arcs, etc. A face is represented by some

description of its surface. Topology records the connectivity of the vertices, edges, and faces by means of pointers in the data structure.

At present, two types of surface representations are used, parametric and polygon.

Parametric modeling represents the exact geometric model with regular shapes or approximates the model using free-form shapes based on polynomial functions. Parametric modeling provides an accurate method of representing objects with curved surfaces. Many types of curves and surface primitives (geometrical objects) exist, and their mathematical representation is based on complex functions (as shown in the figure). The specifics are beyond the scope of this chapter; however, one of their key characteristics is that their shape is determined by the positions of a set of points called "control points." The curves are interpolated (fitted) between this set of points (the curve passes through the points). A characteristic example utilized in the maxillofacial field is the drawing of the panoramic line or the inferior alveolar nerve in various computer-guided surgery applications, by "clicking" (defining) the "control points" through which the respective objects are created. Parametric modeling has been the industry standard for the representation of geometry. The main reason is that it provides flexibility to design a large variety of shapes, without creating too much data and thus large computer files. The primary problem is with branching architecture. For example, the arms branch out of the body, the fingers branch out of the hand, and even the mandible branches out of the head. This is a quite common anatomical feature and is difficult to handle (Fig. 3.3).

A common method of three-dimensional modeling is polygons. A polygon is specified by a list of vertices (points) that define the polygon's region. Several polygons can be combined to represent the object to be modeled. The more complex and accurate the object, the more polygons will be required to model it (Fig. 3.4). Compared to other primitives, polygons have been found to be relatively easy to display, have efficient display algorithms, and are easy to specify, simply by providing a list of points. Polygons are not particularly good for modeling curved faces and require many polygons to do so. This is time-consuming and has an associated computational cost. To overcome this problem, most modeling systems employ shading techniques based on the relative position of external light sources. With careful shading, an object with a relatively coarse surface can appear smooth.

Irrespective of the parametric or polygon modeling chosen, geometric accuracy comes with a price, which is usually increased display time, memory usage, and file size. The required model accuracy is, therefore, application-

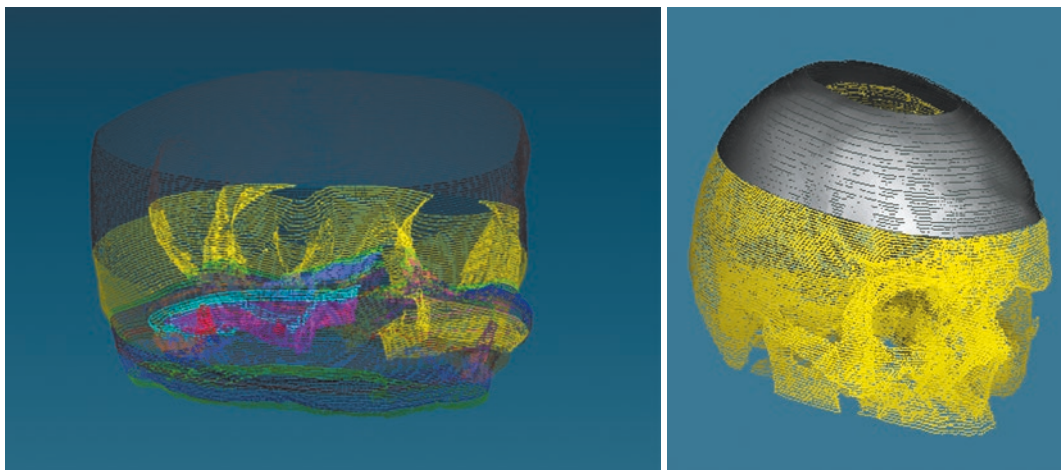

Fig. 3.3 An attempt to model the skull with parametric tools. Due to "branching" geometry, it is necessary to create different sets of lines, upon which surfaces are fit [35]

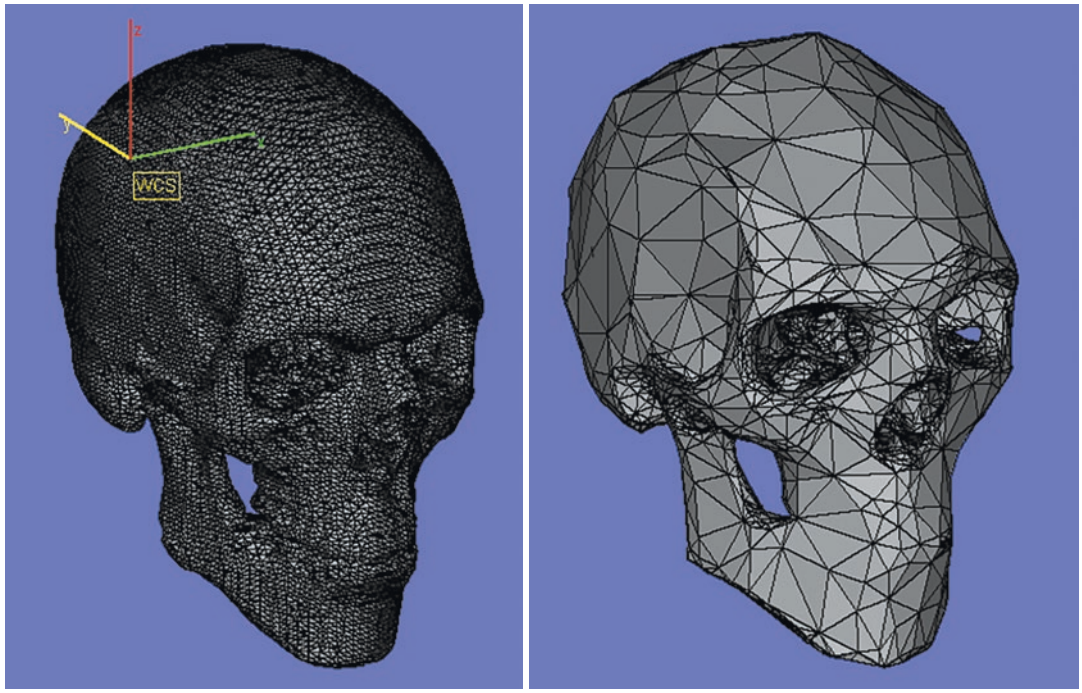

Fig. 3.4 The skull's geometry is represented by polygons. Accuracy is dependent on the total amount of triangles utilized [35]

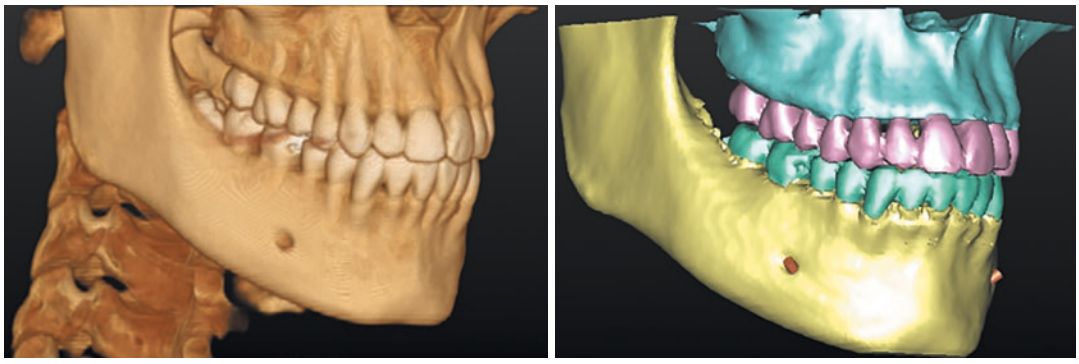

Fig. 3.5 The conversion of a volume representation to a surface representation provides the possibility of "segmenting" the anatomy and hence visualizing this according to the clinician's requirements in order to facilitate diagnosis and preoperative planning

dependent. In a virtual reality environment, it may be possible to represent a sphere as a limited number of polygons; however, in a CAD application, a more precise representation is required.

The computer-aided design (CAD) environment can provide many advantages for modeling of the human anatomy. For achieving this, it is necessary to obtain information on the relevant geometry from medical images. Converting the acquired image data to detailed three-dimensional models can allow the manipulation of the anatomy within a CAD environment in numerous ways (Fig. 3.5). For example, it is possible to perform experimental surgery and evaluate various surgical scenarios. Three-dimensional computer models are also necessary for the biomechanical

study and analysis of anatomical structures as well as for the design of implants. The CAD environment is well-suited and is an effective method to design customized implants based on real anatomical data.

Traditionally, there has been no automatic method of feeding geometry of the anatomy into a CAD environment. The accurate representation of a three-dimensional anatomical model into a CAD format has always been a highly demanding task. Quite often, there has been a need to write specific computer codes in conjunction with commercially available software. The noncompatibility of software and hardware components has been an issue as well as the enormous size of generated computer files and the need for powerful computer systems. In turn, methods of transferring information of medical images to CAD have been inefficient for use within a clinical environment. The need for more automated methods in utilizing geometrical anatomical data within a CAD environment has been well-recognized throughout the years [36, 37].

3.1.3 Finite Element Analysis (FEA)

Finite element analysis (FEA) is a computer-based numerical simulation technique for calculating the strength and behavior of engineering structures. It was first introduced in the 1950s and has been continually developed and improved since then. It is now an extremely sophisticated tool for solving numerous engineering problems and is widely used and accepted in many branches of industry. It can be used in areas as diverse as stress analysis, electromagnetism, heat transfer, vibration, and fluid flow. A computer is required because of the great number of calculations needed to analyze a large structure. As the power of computers has increased, it has become possible to analyze larger and more complex problems.

The basic principles underlying the finite element method are relatively simple. For example, a structure is considered in which the distribution of an unknown variable (such as displacement) is required. In a FEA software package, the structure is broken down into many small, simple blocks known as "elements" (Fig. 3.6), which are interconnected at joints known as "nodes." The variable is assumed to act over each element in a predefined manner. The distribution of the variable across each element may be defined by a polynomial or a trigonometric function. The specific behavior of an individual element can be described with a relatively simple set of equations. After the problem has been "discretized," the governing equations for each element are calculated and then assembled to yield the "system equations." Just as the set of elements would be joined together to build the whole structure, the equations describing the behaviors of the individual elements are joined with an extremely large set of system equations that describe the behavior of the whole structure.

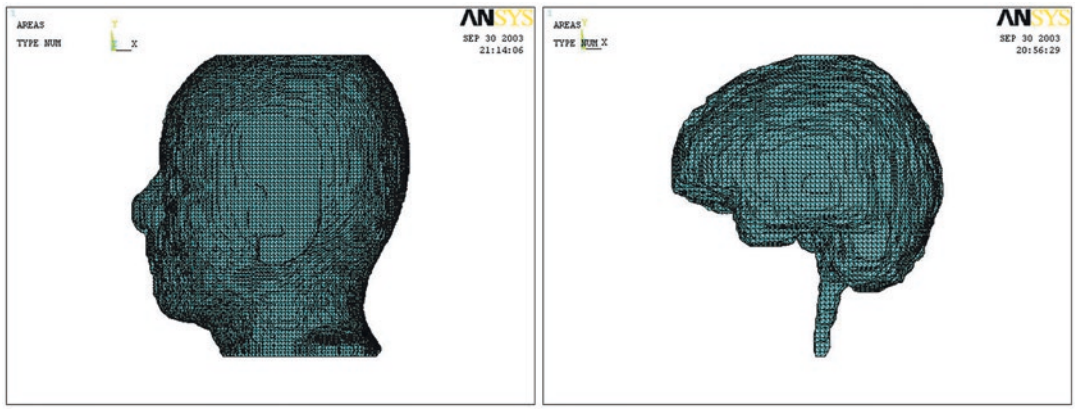

Fig. 3.6 At the preparatory stage of FEA, the anatomy is "broken" down into volume elements [38]

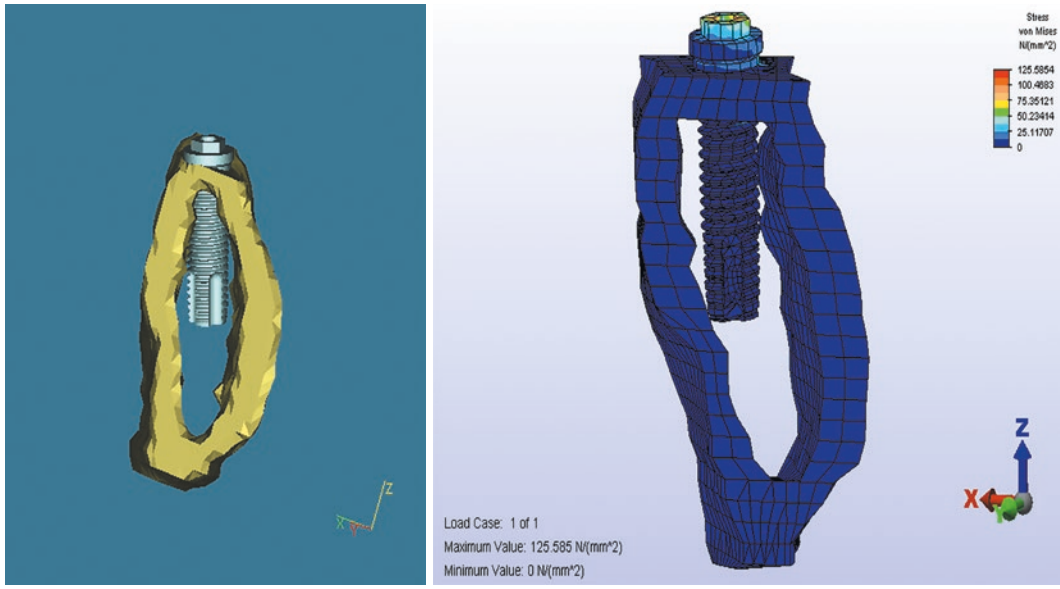

Fig. 3.7 A section of the mandible representing the cortical bone is combined with a dental implant CAD model to study stress distribution in the surrounding area

Finite element analysis (FEA) is a numerical simulation method that has been shown to be applicable to many biomechanical applications and to have considerable potential for studying anatomical functions in a virtual environment [39]. It is especially important though to mention that FEA is fundamentally an approximation. The underlying mathematical model tends to approximate the real physical system. Thus, a good analysis and interpretation of results requires knowing what an acceptable approximation is as well as developing an analysis model that resembles reality as closely as possible. In this respect, medical imaging can provide important information on various anatomical structures and most importantly their geometry as well as their material properties (Fig. 3.7). However, the communication of such information between the image and the FEA software has been exceedingly difficult. The development of accurate three-dimensional models has been a highly demanding task, prone to errors introduced by incorrect representation of geometry and materials. Most biomechanical FEA studies have introduced considerable approximations. In addition, insufficient computer power has also limited the analysis of extensive geometries. Since the early days, well-documented challenges have been posed in biomechanical FEA modeling.

3.1.4 Additive Manufacturing

Additive manufacturing (AM) is a fast and accurate method to develop a three-dimensional object by building up successive thin layers of raw material. Objects are produced from digital 3D files, once they have been designed with CAD, or even simulated by FEA. Physical prototypes of any complexity can usually be built in hours, making significant reductions in the product development cycle. Additive manufacturing (AM) used to be known in the past as rapid prototyping (RP), since it was initiated as a fast and accurate method of building models without investing in production tooling. Prototype models have been used to confirm the basic shape, style, and fit of components, to develop functional parts, and to test new products. The major advantage compared to traditional manufacturing is that objects are developed by adding material rather than by removing material as conventional machining does. Many different processes have been available during the years, using a variety of materials (paper, plastic,

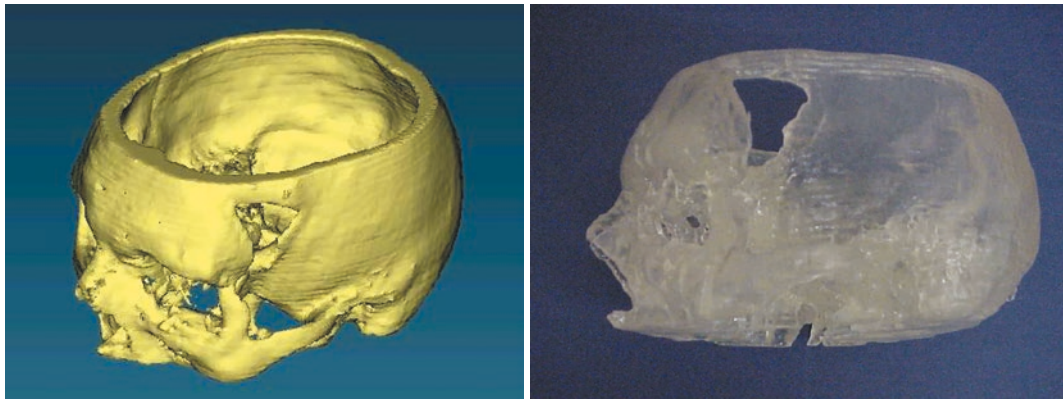

Fig. 3.8 One of the very first anatomical models build through stereolithography [40]

wax, ceramic, metal) that are utilized in a liquid, powder, or solid state. The recent AM systems have combined multiple materials, colors, and textures. Lately, AM, widely also known as 3D printing, has included several established rapid manufacturing techniques. These include, but are not limited to, stereolithography (SLA), selective laser sintering (SLS), and fused deposition modeling (FDM) as well as a multitude of variables or other experimental technologies under development. Each technique has its own limitations and applications in producing models. Additive manufacturing has enormous potential in medical applications [40] (Fig. 3.8), provided that it can also utilize geometrical information of anatomical data in conjunction with CAD and FEA processes.

3.2 The Method of Concurrent Anatomical Engineering

The integration of design and manufacturing technologies enhances the product development process. A new trend has therefore been emerging in industry, a shift toward integrated modeling and production systems. Such a collaborative function of various software or hardware systems is called concurrent engineering. The availability of a virtual computer model in different developmental stages is an essential requirement and a central part of achieving such an integration. Similarly, integrating medical imaging with CAD, FEA, and AM technologies can provide a concurrent engineering process for anatomical modeling as well as considerable benefits for biomedical research, the medical industry, and clinical practice. An efficient concurrent technology interaction can provide engineers and clinicians with sophisticated virtual and physical models of the human anatomy not only to facilitate diagnoses, preoperative planning, and surgical guidance but also to develop customized implants, surgical tools, and, in general, personalized medical devices. Such an integrated approach was proposed for the first time as "biomedical modeling" in medicine by Diamantopoulos in 1999 [38, 41, 42], and, nowadays, the following processes are generally applied (Fig. 3.9):

3.2.1 Image Acquisition

The acquisition of accurate image data is the first and most important step. As described in the earlier section, specific scanning protocols must be followed, and the raw image datasets are digitally exported and saved in a DICOM format.

3.2.2 Image Processing

The acquired DICOM data are imported and processed by specialized image processing software packages with the aim of identifying and extracting specific tissue information. As also explained in the earlier section, every image consists of a collection of different gray values, which are

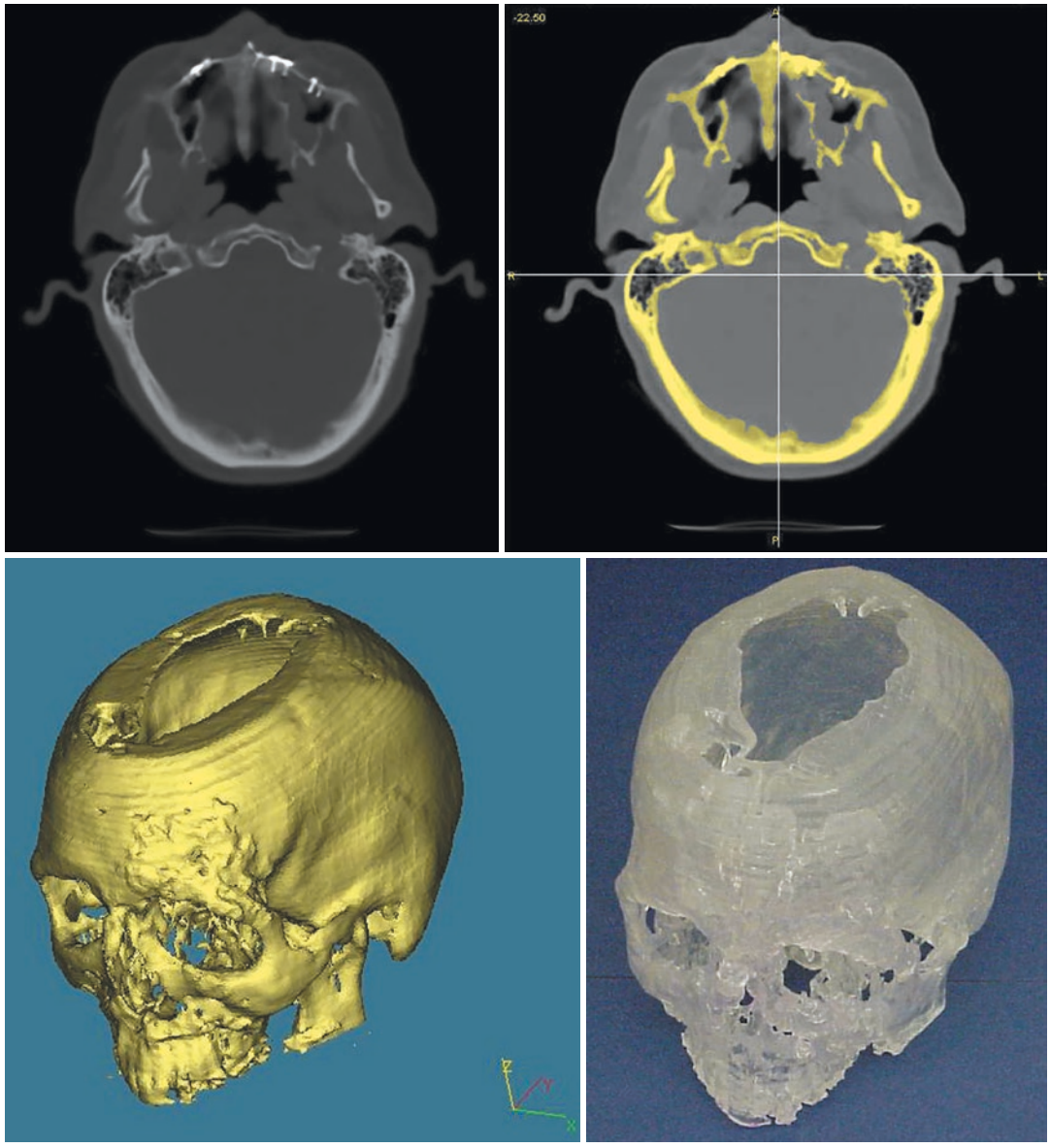

Fig. 3.9 The general process for developing an anatomical virtual or physical model is image acquisition with an appropriate scanning protocol, tissue segmentation, three-dimensional reconstruction, and export to an appropriate format accepted by CAD, FEA, or 3D printing environments [35]

depicted by a sum of pixels or voxels. For instance, in CT, the gray values are expressed in Hounsfield units (HU). By default, the air corresponds to –1024 HU, water to 0 HU, any metal to 3072 HU. In other words, highly dense materials have high values and will be displayed in white, whereas materials that are less dense will have a lower value and will be displayed in variations of gray, and air will be displayed in black. By utilizing this principle and by varying the gray values, a process known as thresholding materials of different densities will stand out; hence, this will permit certain differentiation of the tissues depicted on each image. This process of tissue identification and classification is called segmentation, which is the isolation and grouping of all pixels representing a specific anatomical area of interest.

3.2.3 Interfacing CAD, FEA, and AM

Once the segmentation process is complete, specific algorithms translate the pixel and/or voxel spatial information into the relevant three-dimensional geometrical model, which contains specific points, lines, and surfaces. The representation of this 3D geometry is achieved using polygons, specifically using triangulation algorithms (Fig. 3.10). The most widely known format for describing a three-dimensional surface geometry using triangles is the STL (Standard Tessellation Language) format. This was originally developed for stereolithography, the first additive manufacturing method. However, during the last decade, the STL format has gradually been accepted by most CAD and FEA applications, a useful development that allows the communication and the transfer of the anatomical geometry among various software environments.

By transferring computer models of scanned anatomy to a CAD environment, it is possible to apply various design functions for virtual surgical simulations (measurements, cuts, geometry alterations, procedures) or for creating anatomy-specific implants, instruments, and generally any personalized medical devices. It is also possible to transfer anatomical geometric entities, as well as designed medical devices, to a finite element analysis (FEA) environment for the numerical simulation and validation of the designed parts. Within this virtual environment, different material properties can be assigned, such as for the cancellous and cortical bone, desired loading conditions can be applied so as to study the behavior of the designed part within the intended anatomical structure, and, finally, through additive manufacturing, or 3D printing, it is possible to eventually construct the previously designed and simulated parts in the required material so that they can be used as a test prototype or even as the final functional product.

In general, by following the described methodology, virtual computer modeling and physical production can be combined as required, providing a concurrent engineering approach in the medical industry as well as in clinical practice, with numerous advantages for achieving personalized medicine [35] (Fig. 3.11). The same process has been adapted by many relevant software packages for specific applications such as computer-guided implantology.

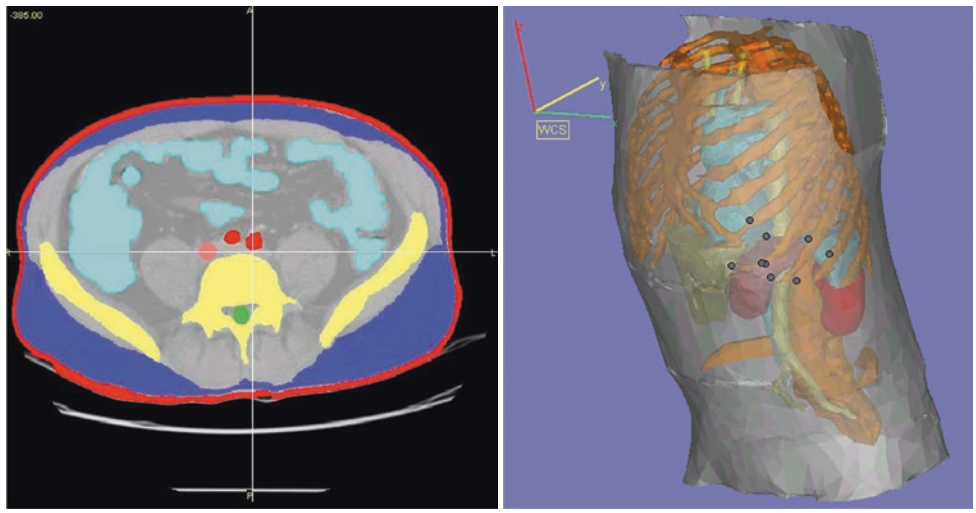

Fig. 3.10 Example segmentation of various anatomical regions using CT images of the torso and the relevant three-dimensional reconstruction using triangulation so that it can be exported as an STL format for subsequent analysis [35]

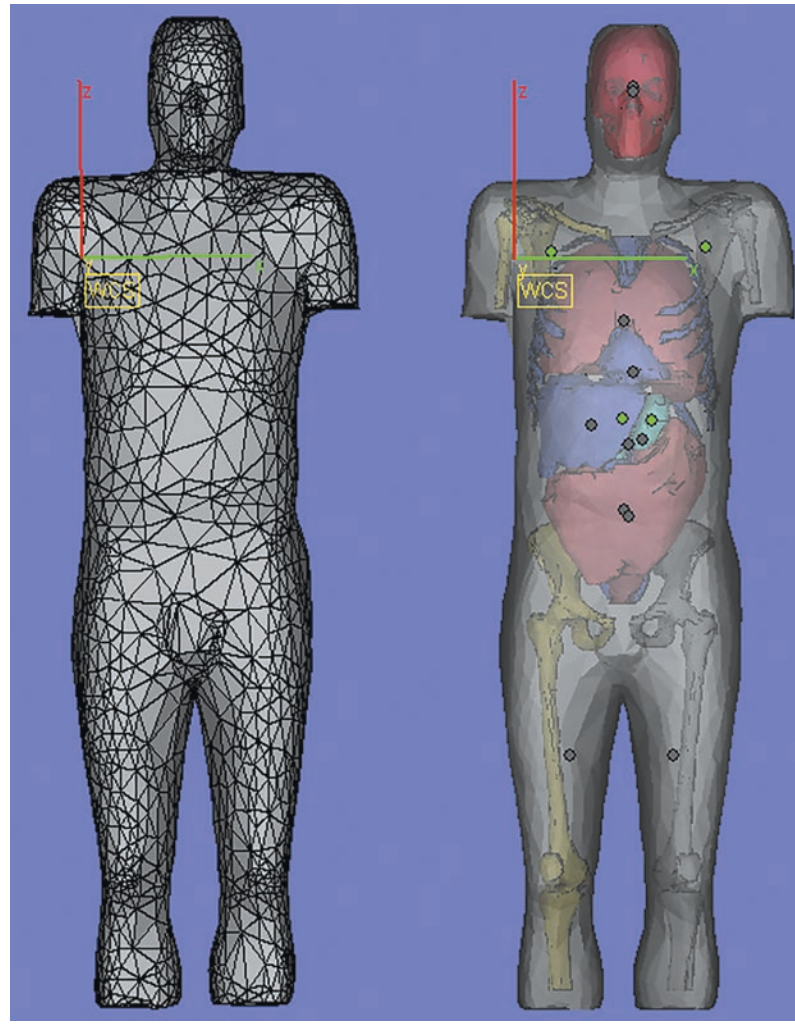

Fig. 3.11 Effective integration of imaging with engineering design and manufacturing allows the possibility of modeling the whole human anatomy [35]

3.3 Potential of Digital Engineering in Clinical Practice

The vast potential of 3D digital technologies, including imaging, design, simulation, and printing, is gradually becoming abundant in clinical practice and in the context of computer-guided surgery. Together, the discussed technologies can provide new virtual and physical tools to better plan and prepare surgical operations (Fig. 3.12). Preoperative visualization and education via the creation of a precise anatomical model may assist the surgeon in the selection of the optimal surgical approach, appropriate implant, and positioning, thereby potentially optimizing patient outcomes and minimizing potential complications. The application of patient-specific guiding instruments, i.e., drilling or osteotomy guides, can also make surgery of complex cases more precise, cost-effective, and possibly easier to perform (Fig. 3.13). In general, replicas of the patient's anatomy, surgical instruments, custom-made implants, and other medical devices may be manufactured in an acceptable matter of time [35, 38, 40–43] (Fig. 3.14).

Further implementation of these technologies into any clinical field is to be expected. If the operations can be carried out more successfully, then reduced risks, reduced patient suffering, and improvements in the quality of the results are to be expected, in addition to less costs associated with postoperative treatment.

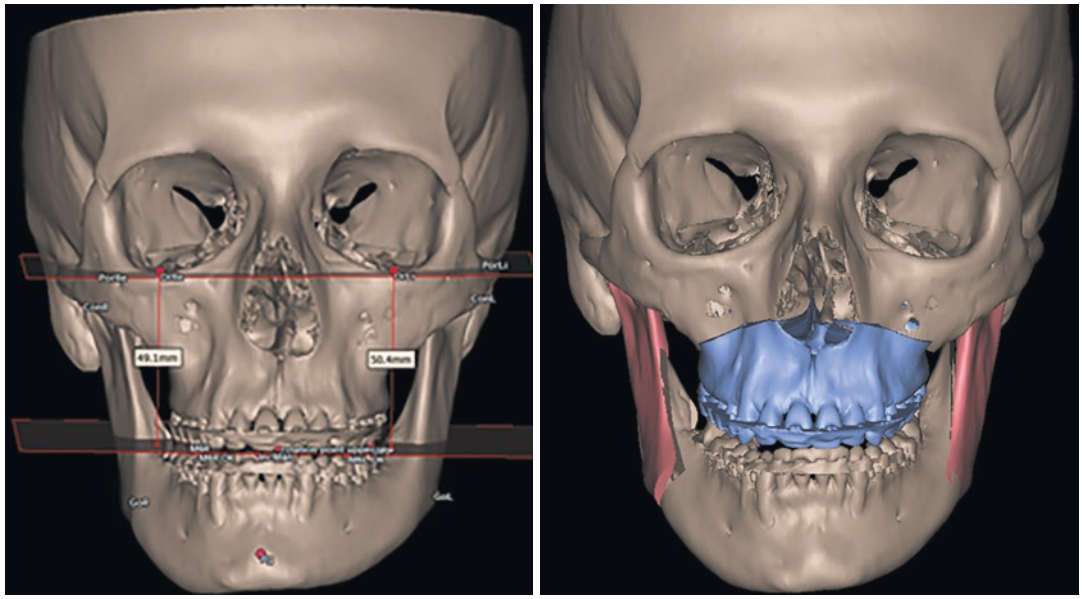

Fig. 3.12 Virtual preoperative plan of orthognathic surgery. (Courtesy of Drs. Ana Tache and Maurice Mommaerts, European Face Centre, Brussels, Belgium)

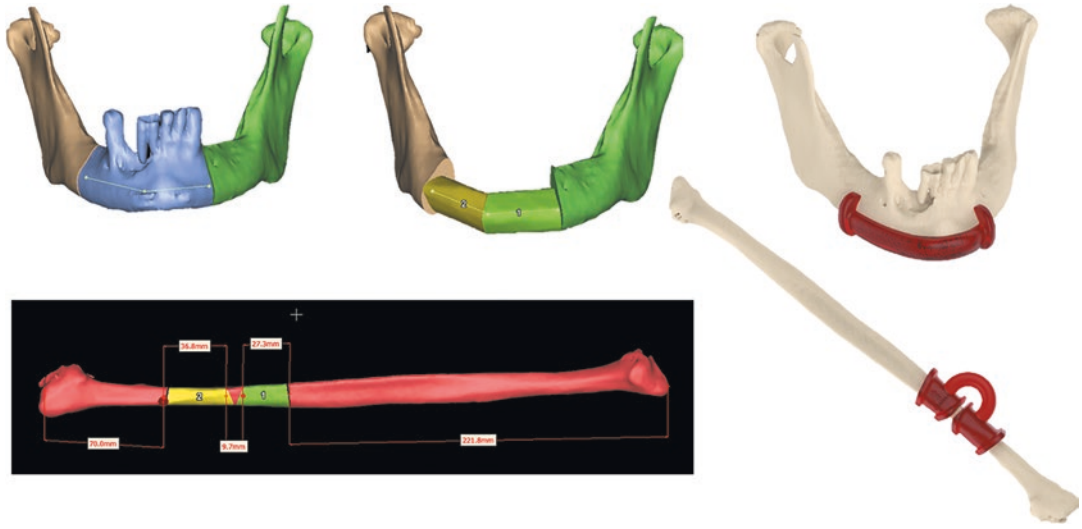

Fig. 3.13 Planning of a fibula transplant for mandibular segment reconstruction. (Courtesy of Drs. Beckers and Mommaerts, European Face Centre, Brussels, and Dr. Beckers and Ruben Vande Sande, CADskills BV, Ghent, Belgium)

However, since patient-specific implants and instruments are more expensive, further research should also focus on comparing patient outcomes in systematically using 3D technology versus conventional preoperative planning to justify their use in routine surgical practice and therefore lowering the cost. The cost benefit of using such technologies in terms of money saved, surgical hours reduced, enhanced patient services, and speeded recovery should be quantified. It is also imperative that the clinicians and technicians involved become acquainted with the technology in order to promote further implementation.

In general, the gradual integration of medical imaging with modern three-dimensional (3D) digital engineering technologies during that last

two decades has been revolutionizing clinical practice in all medical disciplines [35, 38, 40–43]. Several clinical applications including preoperative planning, surgical simulation, patient-specific instrumentation, and implants would have been impossible otherwise (Fig. 3.15).

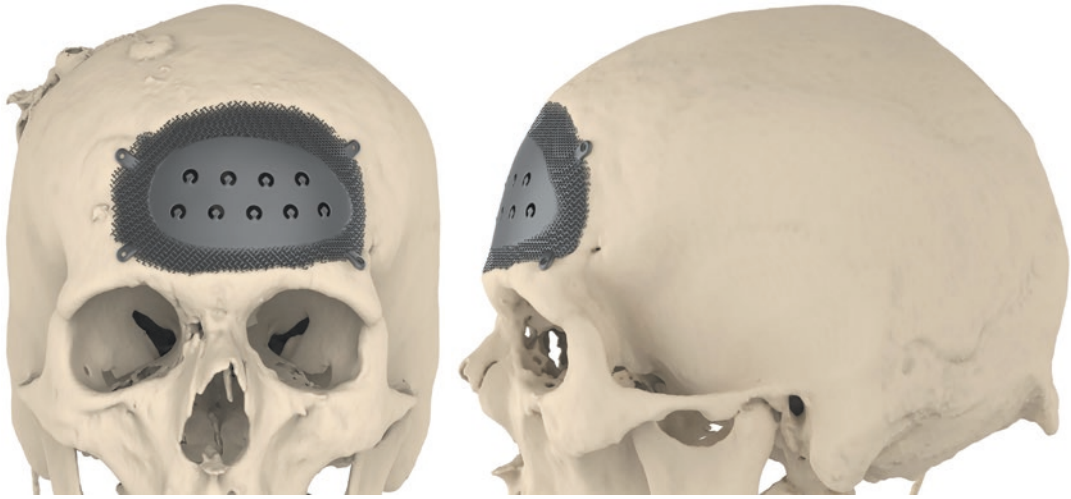

Fig. 3.14 Design of s customized CeTi cranioplasty implant. (Courtesy of Ruben Vande Sande, CADskills BV, Ghent, and Dr. F. De Waele, University of Ghent, Belgium)

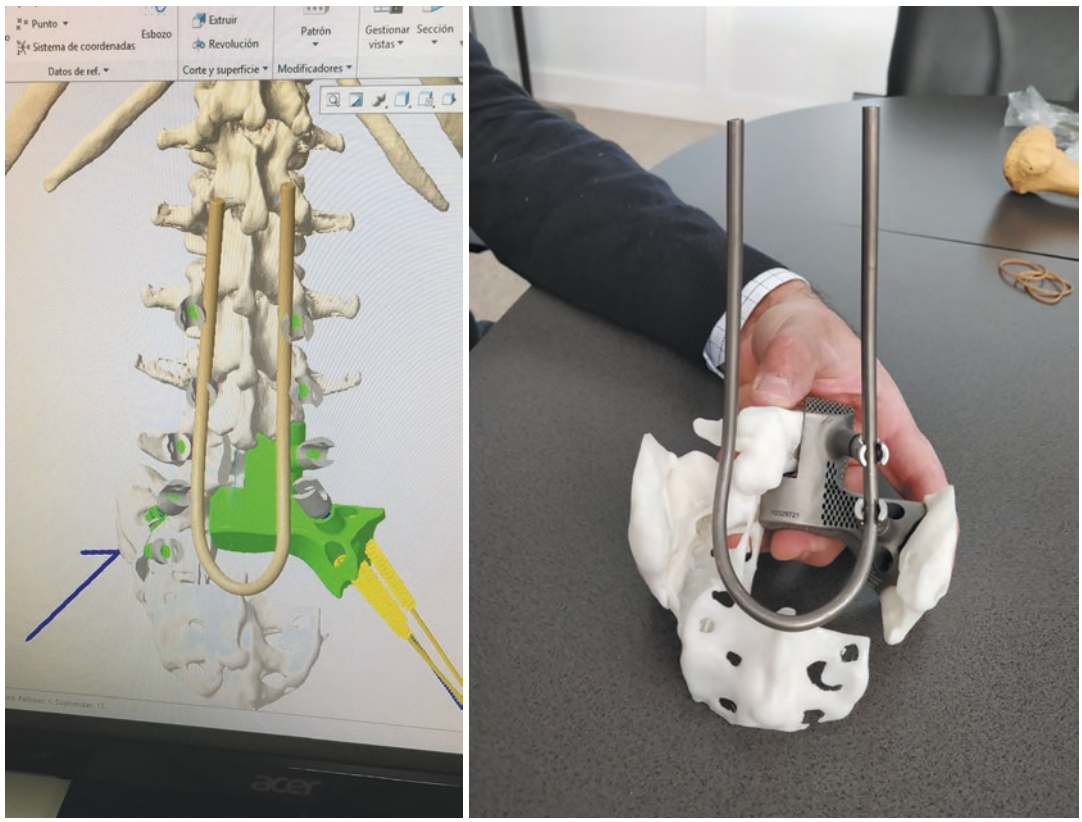

Fig. 3.15 Design and additive manufacturing of a custom-made implant for spine reconstruction after sacrum resection and L5 hemivertebrectomy. (Courtesy of Dr. Alessandro Gasbarrini, Rizzoli Orthopaedic Institute, Bologna, Italy)

In the future, it should be expected that E-engineering and virtual reality (VR) possibilities will be integrated in such applications. Such facilities will provide high levels of interactivity between bioengineers and surgeons, not only with a sense of immersion and an improvement of interaction over the design and manufacturing of medical devices but also on the actual surgical procedures in conjunction with robotics. In addition, while 3D technologies have already been used for printing biological scaffolds and successfully tested in vitro and in vivo animal studies, human trials will also be performed for establishing bioprinting.

References

1. Radon J. Uber die eestimmung von funktionen durch ihre integralwerte langs gewisser mannigfaltigkeite. Ber Verh Sachs Akad Wiss Leipzig Math Phys. 1917;69:262–77.
2. Hounsfield GN. Computerised transverse axial scanning (tomography). Part 1: description of system. Br J Radiol. 1973;46:1016–22.
3. Tetel'baum SI. About a method of obtaining volume images with the help of x-rays. Bull Kiev Polytechnic Inst. 1957;22:154–60.
4. Korenblyum BI, Tetel'baum SI, Tyutin AA. About one scheme of tomography. Bull Inst Higher Educ Radiophys. 1958;1(3):151–7.
5. Cormack AM. Early two-dimensional reconstruction and recent topics stemming from it (Nobel Prize Lecture). Science. 1980;209:1482–6.
6. Lindley A. Practical image processing in C. Englewood Cliffs, NJ: Prentice Hall; 1983.
7. Tonkopi E, Duffy S, Abdolell M, Manos D. Diagnostic reference levels and monitoring practice can help reduce patient dose from CT examinations. Am J Roentgenol. 2017;208:1073–81. https://doi.org/10.2214/AJR.16.16361.
8. Bauhs JA, Vrieze TJ, Primak AN, et al. CT dosimetry: comparison of measurement techniques and devices. Radiographics. 2008;28:245–53.
9. Widmann G, Torbica P, Verius M, Jaschke W. Röntgenstrahlenschutz kompakt. Informationen aus Orthod Kieferorthopädie. 2020;52:232–6. https://doi.org/10.1055/a-1200-5809.
10. Christner JA, Kofler JM, McCollough CH. Estimating effective dose for CT using dose-length product compared with using organ doses: consequences of adopting international commission on radiological protection publication 103 or dual-energy scanning. Am J Roentgenol. 2010;194:881–9. https://doi.org/10.2214/AJR.09.3462.
11. Deak PD, Smal Y, Kalender WA. Multisection CT protocols: sex- and age-specific conversion factors used to determine effective dose from dose-length product. Radiology. 2010;257:158–66. https://doi.org/10.1148/radiol.10100047.
12. Ludlow JB, Timothy R, Walker C, et al. Effective dose of dental CBCT—a meta analysis of published data and additional data for nine CBCT units. Dentomaxillofacial Radiol. 2015;44:20140197.
13. McCollough CH, Chen GH, Kalender W, et al. Achieving routine submillisievert CT scanning: report from the summit on management of radiation dose in CT. Radiology. 2012;264:567–80. https://doi.org/10.1148/radiol.12112265.
14. Duan X, Wang J, Christner JA, et al. Dose reduction to anterior surfaces with organ-based tube-current modulation: evaluation of performance in a phantom study. Am J Roentgenol. 2011;197:689–95. https://doi.org/10.2214/AJR.10.6061.
15. Widmann G, Dalla Torre D, Hoermann R, et al. Ultralow-dose computed tomography imaging for surgery of midfacial and orbital fractures using ASIR and MBIR. Int J Oral Maxillofac Surg. 2015;44:441–6. https://doi.org/10.1016/j.ijom.2015.01.011.
16. Widmann G, Juranek D, Waldenberger F, et al. Influence of ultra-low-dose and iterative reconstructions on the visualization of orbital soft tissues on maxillofacial CT. Am J Neuroradiol. 2017;38:1630–5. https://doi.org/10.3174/ajnr.A5239.
17. Al-Ekrish AA, Alzahrani A, Zaman MU, et al. Assessment of potential reduction in multidetector computed tomography doses using FBP and SAFIRE for detection and measurement of the position of the inferior alveolar canal. Oral Surg Oral Med Oral Pathol Oral Radiol. 2020;129:65–71.e7. https://doi.org/10.1016/j.oooo.2019.09.002.
18. Al-Ekrish AA, Al-Shawaf R, Schullian P, et al. Validity of linear measurements of the jaws using ultralow-dose MDCT and the iterative techniques of ASIR and MBIR. Int J Comput Assist Radiol Surg. 2016;11:1791–801. https://doi.org/10.1007/s11548-016-1419-y.
19. Al-Ekrish AA, Al-Shawaf R, Alfaleh W, et al. Comparability of dental implant site ridge measurements using ultra-low-dose multidetector row computed tomography combined with filtered back-projection, adaptive statistical iterative reconstruction, and model-based iterative reconstruction. Oral Radiol. 2018;35(3):280–6. https://doi.org/10.1007/s11282-018-0350-z.
20. Al-Ekrish AA, Alfadda SA, Ameen W, et al. Accuracy of computer-aided design models of the jaws produced using ultra-low MDCT doses and ASIR and MBIR. Int J Comput Assist Radiol Surg. 2018;13:1853–60. https://doi.org/10.1007/s11548-018-1809-4.
21. Widmann G, Fasser M, Schullian P, et al. Substantial dose reduction in modern multi-slice spiral computed tomography (MSCT)-guided craniofacial and skull base surgery. RoFo Fortschritte auf dem Gebiet der Rontgenstrahlen und der

Bildgeb Verfahren. 2012;184:136–42. https://doi.org/10.1055/s-0031-1281971.
22. Eggers G, Klein J, Welzel T, Mühling J. Geometric accuracy of digital volume tomography and conventional computed tomography. Br J Oral Maxillofac Surg. 2008;46:639–44. https://doi.org/10.1016/j.bjoms.2008.03.019.
23. Loubele M, Maes F, Schutyser F, et al. Assessment of bone segmentation quality of cone-beam CT versus multislice spiral CT: a pilot study. Oral Surg Oral Med Oral Pathol Oral Radiol Endodontol. 2006;102:225–34. https://doi.org/10.1016/j.tripleo.2005.10.039.
24. Liang X, Lambrichts I, Sun Y, et al. A comparative evaluation of cone beam computed tomography (CBCT) and multi-slice CT (MSCT). Part II: on 3D model accuracy. Eur J Radiol. 2010;75:270–4. https://doi.org/10.1016/j.ejrad.2009.04.016.
25. D'haese J, Van De Velde T, Elaut L, De Bruyn H. A prospective study on the accuracy of mucosally supported stereolithographic surgical guides in fully edentulous maxillae. Clin Implant Dent Relat Res. 2012;14:293–303. https://doi.org/10.1111/j.1708-8208.2009.00255.x.
26. Valente F, Schiroli G, Sbrenna A. Accuracy of computer-aided oral implant surgery: a clinical and radiographic study. Int J Oral Maxillofac Implants. 2009;24:234–42.
27. Vasak C, Watzak G, Gahleitner A, et al. Computed tomography-based evaluation of template (NobelGuide TM)-guided implant positions: a prospective radiological study. Clin Oral Implants Res. 2011;22:1157–63. https://doi.org/10.1111/j.1600-0501.2010.02070.x.
28. Van Assche N, Van Steenberghe D, Quirynen M, Jacobs R. Accuracy assessment of computer-assisted flapless implant placement in partial edentulism. J Clin Periodontol. 2010;37:398–403. https://doi.org/10.1111/j.1600-051X.2010.01535.x.
29. Di Giacomo GA, da Silva JV, da Silva AM, et al. Accuracy and complications of computer-designed selective laser sintering surgical guides for flapless dental implant placement and immediate definitive prosthesis installation. J Periodontol. 2012;83:410–9. https://doi.org/10.1902/jop.2011.110115.
30. Eggers G, Senoo H, Kane G, Mühling J. The accuracy of image guided surgery based on cone beam computer tomography image data. Oral Surg Oral Med Oral Pathol Oral Radiol Endodontol. 2009;107(3):e41–8. https://doi.org/10.1016/j.tripleo.2008.10.022.
31. Widmann G, Zangerl A, Schullian P, et al. Do image modality and registration method influence the accuracy of craniofacial navigation? J Oral Maxillofac Surg. 2012;70:2165–73. https://doi.org/10.1016/j.joms.2011.08.026.
32. Wagner A, Schicho K, Kainberger F, et al. Quantification and clinical relevance of head motion during computed tomography. Invest Radiol. 2003;38:733–41. https://doi.org/10.1097/01.rli.0000084889.92250.b0.
33. Al-Ekrish A, Widmann G, Alfadda S. Revised, computed tomography–based Lekholm and Zarb jawbone quality classification. Int J Prosthodont. 2018;31:342–5. https://doi.org/10.11607/ijp.5714.
34. Al-Ekrish AA, Alfadda SA, Tamimi D, et al. Do ultralow multidetector computed tomography doses and iterative reconstruction techniques affect subjective classification of bone type at dental implant sites? Int J Prosthodont. 2018;31(5):465–70. https://doi.org/10.11607/ijp.5773.
35. Diamantopoulos P, et al. Integrating medical imaging, FEA, CAD and rapid prototyping. In: Middleton J, Jones MJ, Pande G, editors. Computer methods in biomechanics and biomedical engineering, vol. 3. Amsterdam: Gordon & Breach; 2001. p. 501–8.
36. Viceconti M, Zannoni C, Testi D, et al. A new method for the automatic mesh generation of bone segments from CT data. J Med Eng Technol. 1999;23(2):77–81.
37. Zannoni C, Cappello A, Viceconti M. Optimal CT scanning plan for long-bone 3-D reconstruction. IEEE Trans Med Imaging. 1998;17(4):663–6.
38. Diamantopoulos P, et al. Interfacing data between medical imaging, FEA, CAD and rapid prototyping: a practical methodology. In: Proceedings of the annual meeting of the Institute of Physics & Engineering in Medicine, Nottingham, September 1999. London: IPEM; 1999. p. 2.
39. Huiskes R, Hollister SJ. From structure to process, from organ to cell: recent developments of FE-analysis in orthopaedic biomechanics. J Biomech Eng. 1993;115(4B):520–7.
40. Diamantopoulos P, et al. Medical rapid prototyping. In: UK Radiological Congress, London, May 2001. London: British Institute of Radiology; 2001. p. 52.
41. Diamantopoulos P. Medical imaging, CAD, FEA, and rapid prototyping: an integrated approach. Presented at measurements and simulations in orthopaedic biomechanics meeting, Royal College of Surgeons, London, June 1999; 1999.
42. Diamantopoulos P. Interfacing medical imaging data to FEA, CAD and rapid prototyping. Paper presented at the international conference of computer methods in biomechanics and biomedical engineering, Lisbon, October 1999; 1999.
43. Diamantopoulos P, et al. Introducing biomechanical computational methods into a hospital environment. In: Proceedings of the 12th conference of the European Society of Biomechanics, Dublin, August 2000. Royal Academy of Medicine; 2000. p. 405.